# Mound formation in surface growth under shadowing

M. Pelliccione, T. Karabacak, C. Gaire, G.-C. Wang, and T.-M. Lu
*Department of Physics, Applied Physics, and Astronomy, and Center for Integrated Electronics, Rensselaer Polytechnic Institute, Troy, New York 12180-3590, USA*

(Received 16 May 2006; revised manuscript received 21 July 2006; published 20 September 2006)

In this paper we report on the morphological evolution of thin films grown by commonly employed deposition techniques, such as sputtering and chemical vapor deposition. In these deposition techniques, an angular distribution of incident particle flux leads to the shadowing effect, which often plays an important role in defining the growth front morphology. We show both by simulations and experiments that a mounded structure can be formed with a characteristic length scale, or "wavelength" $\lambda$, which describes the separation of the mounds. We also show that the temporal evolution of $\lambda$ is distinctly different from that of the mound size or lateral correlation length $\xi$. The wavelength grows as a function of time in a power-law form, $\lambda \sim t^p$, where $p \approx 0.5$ for a wide range of growth conditions, while the mound size grows as $\xi \sim t^{1/z}$, where $1/z$ varies depending on growth conditions. The existence of these two length scales and their different growth rates leads to a breakdown of the self-affine and dynamic scaling hypotheses that have been used to describe many surface growth phenomena in the past.

DOI: 10.1103/PhysRevB.74.125420 PACS number(s): 68.55.−a, 81.15.−z

## I. INTRODUCTION

Thin film surface morphology controls many important physical and chemical properties of the films. It is therefore of great interest to understand and control the evolution of the surface morphology during thin film growth. The formation of a growth front is a complex phenomenon and very often occurs far from equilibrium. When atoms are deposited on a surface, atoms do not arrive at the surface at the same time uniformly across the surface. This random fluctuation, or noise, which is inherent in the process, may create surface growth front roughness. The noise competes with surface smoothing processes, such as surface diffusion, to form a rough morphology if the experiment is performed at either a sufficiently low temperature or at a high growth rate.

A conventional statistical mechanics treatment cannot be used to describe this complex phenomenon. About two decades ago, a dynamic scaling approach[1,2] was proposed to describe the morphological evolution of a growth front. Since then, numerous modeling and experimental works have been reported based on this dynamic scaling analysis.[3,4] In this analysis, the surface is described by the equal-time height-height correlation function $H(\mathbf{r})$, defined as $H(\mathbf{r}) \equiv \langle [h(\mathbf{r}) - h(\mathbf{0})]^2 \rangle$. Here, $h(\mathbf{r})$ is the surface height at a position $\mathbf{r}$ on the surface. The angular brackets denote a statistical average. The dynamic scaling hypothesis requires that $H(r) \sim r^{2\alpha}$ for $r \ll \xi$ and $H(r) \sim 2w^2$ for $r \gg \xi$, where $\xi$ is the lateral correlation length, $w$ is the interface width or root-mean-square (rms) roughness, and $\alpha$ is the roughness exponent, which describes how "wiggly" the local surface is. Both $w$ and $\xi$ grow as a power law in time, $w \sim t^{\beta}$ and $\xi \sim t^{1/z}$, where the exponents $\beta$ and $z$ are called the growth exponent and dynamic exponent, respectively. Dynamic scaling requires $z = \alpha/\beta$.[1]

One notes that in the dynamic scaling hypothesis, the surface vertical direction does not scale the same way as does the lateral direction. It is therefore not a self-similar surface, but rather a self-affine surface. An important feature of a self-affine surface is that the height-height correlation function reaches a constant value (equal to $2w^2$) at a large distance at a given time. This distance defines the lateral correlation length $\xi$, beyond which the surface height fluctuations are not correlated. This means that there is no long-range characteristic length scale involved; the surface height fluctuation is random beyond the correlation length. This assumption is valid for a number of surface growth models[3,4] where local smoothing effects, such as surface diffusion, are operative to compete with the noise.

However, in practice, in many common modern deposition techniques, including sputter deposition and chemical vapor deposition (CVD), nonlocal effects, such as shadowing,[5–7] along with the redistribution of atoms reflected from the surface due to a nonunity sticking coefficient[8] can play an important role in defining the surface morphology during growth. We show that these nonlocal effects give rise to a mound structure that cannot be described within the context of self-affinity. A mound structure possesses a characteristic long-range length scale $\lambda$, or wavelength, that is a measure of the average distance between mounds. [This mound structure is unrelated to that created by step-barrier diffusion in molecular beam epitaxy (MBE).[9] Since mounds in MBE are formed by a local growth effect, the growth dynamics can be described using a local continuum equation,[10] whereas the growth effects considered in this paper are nonlocal. The wavelength $\lambda$ for surfaces in MBE has been shown to behave as a power law $\lambda \sim t^p$, where $p$ ranges from 0.16 to 0.26 (Refs. 11 and 12).] The quasiperiodic behavior quantified by this wavelength is distinctly different from the behavior of the mound size, or the lateral correlation length $\xi$. Using Monte Carlo (MC) simulations and experimentally deposited surfaces, we show that the separation of mounds grows as a function of time in a power-law form, $\lambda \sim t^p$, where $p \approx 0.5$ for a wide range of deposition conditions under nonlocal shadowing and reemission effects. On the other hand, the growth exponent $1/z$ that is associated with the growth of the mound size, $\xi \sim t^{1/z}$, does depend on deposition conditions, such as the sticking coeffi-

 

cient. We show that deviation in the growth of the mound separation and the mound size leads to a breakdown of the self-affinity and dynamic scaling of the system. A brief account of this phenomenon has been reported earlier,[13] and the present paper presents a detailed description of this work with additional simulation and experimental data.

## II. SCALING HYPOTHESES

Before mounded surfaces are shown to deviate from dynamic scaling and self-affinity under the shadowing effect, it will be helpful to review the properties of self-affinity and dynamic scaling so that one can gain insight into the salient characteristics of mound formation under shadowing.

### A. Self-affine scaling

Consider a surface-height profile $h(r)$. This surface is said to be self-affine if, for an arbitrary scale factor $\epsilon > 0$,[4]

$$h(r) \sim \epsilon^{-\alpha} h(\epsilon r), \tag{1}$$

where the symbol $\sim$ denotes a similar statistical behavior. The roughness exponent $\alpha$ characterizes the short-range roughness of a self-affine surface, with larger values of $\alpha$ representing a smoother local surface profile.

The power spectral density function (PSD) of a surface profile is a Fourier transform of the surface heights. A suitable model for the PSD of a self-affine surface is given by[14]

$$P(k_{\|}) = \frac{4\pi\alpha w^2 \xi^2}{(1 + k_{\|}^2 \xi^2)^{1+\alpha}}, \tag{2}$$

where $k_{\|}$ is the parallel component of the wave vector $\mathbf{k}$. Note that this PSD has no characteristic peak, which allows for the scaling definition of a self-affine surface.[14] A characteristic peak in the PSD implies that there is a characteristic length scale on the surface that will change on rescaling, breaking the scaling behavior of the surface. Since self-affine surfaces have no such peak in their PSD, the scaling definition holds.

### B. Dynamic scaling

A surface profile is said to exhibit dynamic scaling if the surface height profile can be scaled in time. For a self-affine surface, this gives[15]

$$h(r,t) \sim \epsilon^{-\alpha} h(\epsilon r, \epsilon^z t), \tag{3}$$

where $z$ is the dynamic exponent. Under dynamic scaling, increasing the time by a factor $\epsilon$ increases the horizontal length scale by a factor $\epsilon^{1/z}$. Thus, the lateral correlation length, which is a function of the horizontal correlations on the surface, must evolve as

$$\xi(t) \sim t^{1/z}. \tag{4}$$

Similarly, increasing the time by a factor $\epsilon$ changes the vertical length scale by a factor $\epsilon^{\alpha/z}$. Since the interface width is a function of the vertical height profile of the surface, the interface width must evolve as

$$w(t) \sim t^{\alpha/z}. \tag{5}$$

The interface width is commonly defined as evolving with an exponent $\beta$, which, when compared to Eq. (5), gives the well-known relationship between the scaling exponents under dynamic scaling, $z = \alpha/\beta$.

Dynamic scaling predicts that all parameters that measure the surface are related to one another because the surface profile scales as a whole in time. Thus, one consequence of dynamic scaling is the time-dependent scaling of surface correlation functions. Time-dependent scaling implies that correlation functions measured at different deposition times can be collapsed onto one another by a suitable rescaling of the axes of the plots. Since the overall behavior of a surface scales in time under dynamic scaling, a function that measures correlations on the surface should exhibit a similar time-dependent scaling behavior. For example, for the PSD of a self-affine surface from Eq. (2), scaling the horizontal wave number axis $k$ by a factor $[\xi(t)]^{-1}$ and the vertical PSD axis by a factor $[w(t)\xi(t)]^{-2}$ gives a time-independent scaling form $Q(k_{\|})$ for the PSD of a self-affine surface

$$Q(k_{\|}) = \frac{4\pi\alpha}{(1 + k_{\|}^2)^{1+\alpha}}. \tag{6}$$

Clearly, if the PSD of a surface does not obey time-dependent scaling, it would imply that the surface does not obey dynamic scaling. Thus, one way to test the dynamic scaling hypothesis for mounded surfaces is to investigate the time-dependent scaling behavior of the PSD for a mounded surface.

## III. MOUNDED SURFACES

When dealing with self-affine surfaces, there is only one lateral length scale, the lateral correlation length, beyond which surface heights are uncorrelated on the average. However, because self-affine surfaces have a unique scaling behavior, the magnitude of the lateral correlation can be rescaled, which implies that the lateral correlation length is not a true characteristic length scale of the surface, but rather a relative length scale. Surfaces that possess a characteristic length scale are called mounded surfaces. Clearly, from the above heuristic argument, mounded surfaces are not self-affine. This can be mathematically shown using the power spectral density function (PSD). If a surface possesses a characteristic length scale, it would result in a frequency peak in the PSD spectrum. From Eq. (2), the PSD of a self-affine surface has no peak and, as a result, is not mounded. Surfaces that are mounded are said to exhibit wavelength selection. Various growth processes can lead to mounded surfaces, including the step-barrier diffusion effect in MBE. Of interest in this work are the nonlocal shadowing and reemission effects.

### A. Shadowing

In many common thin film growth techniques, such as sputter deposition and chemical vapor deposition (CVD), the growth dynamics often involve nonlocal growth effects. The

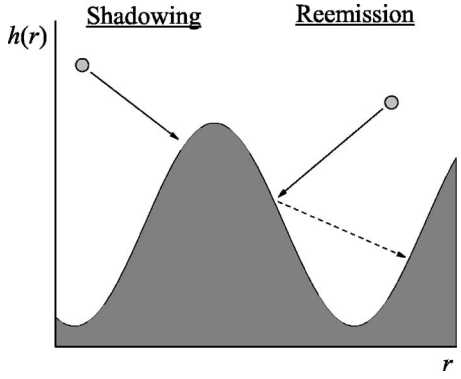


FIG. 1. Diagram of the nonlocal shadowing and reemission effects (Ref. 18). Shadowing occurs when tall surface features block particle flux from valleys. The reemission effect allows otherwise shadowed surface features to receive particle flux.

primary nonlocal effect is the shadowing effect,[6,8] where taller surface features block incoming flux from reaching lower lying areas of the surface. A schematic diagram of the shadowing effect is seen in Fig. 1. The shadowing effect is active because, in sputter deposition and CVD, the incoming flux has an angular distribution. This allows taller surface features to grow at the expense of shorter ones, leading to a competition between different surface features for particle flux. This competition ultimately leads to a mounded surface as shorter surface features receive little or no particle flux and "die out." Shadowing is an inherently nonlocal process because the shadowing of a surface feature depends on the heights of all other surface features, not just close, or local, ones.

### B. Reemission

The formation of mounds due to the shadowing effect can be hindered by the reemission of particles during deposition. The reemission effect allows particles to "bounce around" before they settle at appropriate sites on the surface.[8] A diagram of the reemission effect is seen in Fig. 1. Reemitted particles serve to change the overall particle flux incident on the surface, allowing previously shadowed surface features to receive particle flux. To describe the reemission effect, a sticking coefficient ($s_0$) is used that represents the probability a particle will stick to the surface when it first strikes. Higher-order sticking coefficients ($s_{n>0}$) represent the probability a particle will stick having been reemitted $n$ times. During deposition, shadowing tends to roughen the surface and reemission tends to smoothen the surface.[17] Thus, growth under perfect shadowing would correspond to no reemission ($s_0=1$).

### C. Length scales λ and ξ

Even though there is a characteristic length scale for a mounded surface, the wavelength λ, the lateral correlation length $\xi$ is still well defined. The lateral correlation length is the length beyond which surface heights are not significantly correlated. For a mounded surface, this implies that the lateral correlation length is a measure of the size of the mounds. In some contexts, the lateral correlation length for a mounded surface is called the mound size, denoted by $\zeta$. The wavelength λ is related to the frequency peak in the PSD spectrum, and since the frequency peak in the PSD spectrum is a measure of the periodicity of mounds, this implies that the wavelength λ is a measure of the average distance between mounds. Note that the lateral correlation length $\xi$ and the wavelength λ are defined differently and are not necessarily equal. They only must satisfy the relation $\xi \leq \lambda$ because mounds are separated by at least their size; only if mounds grow next to one another would it imply that $\xi=\lambda$. Figure 2 shows the definition of the lateral correlation length $\xi$ and the wavelength λ for a (1+1)-dimensional mounded surface. This difference between λ and $\xi$ is the basis for the breakdown of dynamic scaling in mounded surfaces grown under the shadowing effect.

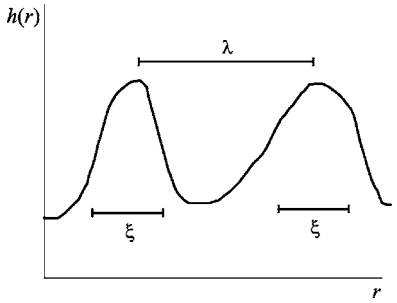


FIG. 2. Definition of the wavelength λ and the lateral correlation length $\xi$ for a mounded surface. In general, the wavelength is not equal to the lateral correlation length, as seen in the figure.

### D. Power spectral density function

The PSD of a mounded surface in 2+1 dimensions can be represented by, for $\alpha=1$,[14]

$$P(k) = \frac{w^2\xi^2}{2} \exp\left[-\frac{(4\pi^2 + k^2\lambda^2)\xi^2}{4\lambda^2}\right] I_0\left(\frac{\pi k \xi^2}{\lambda}\right), \qquad (7)$$

where $I_0(x)$ is the zeroth-order modified Bessel function of the first kind. The roughness exponent $\alpha$ is set equal to 1 in order to obtain a closed-form expression for the PSD, but when $\alpha \neq 1$, the PSD has the same characteristic shape. The peak position is given by $k_m=2\pi\lambda^{-1}$. The peak position of the PSD is often found to behave as a power law in time, $k_m \sim t^{-p}$, where $p$ is the wavelength exponent. This implies a similar behavior for the wavelength

$$\lambda \sim t^p. \qquad (8)$$

In addition, the full width at half maximum (FWHM) of the PSD of a mounded surface is inversely proportional to the lateral correlation length; FWHM $\propto \xi^{-1}$. This property is not obvious from the functional form of the PSD, but can be shown through a numerical analysis.[14] It is a reasonable conclusion because the FWHM for a self-affine PSD is also inversely proportional to the lateral correlation length, as is evident from Eq. (2).

### E. Breakdown of dynamic scaling

The time-dependent scaling behavior of a PSD is related to the overall dynamic scaling behavior of the surface profile, as was shown in Sec. II B. In attempting to find scale factors to remove the time dependence from Eq. (7), we find that, in general, the time dependence cannot be removed from the PSD. Recall that the parameters $w(t)$, $\xi(t)$, and $\lambda(t)$ all change with time and are not necessarily related. For example, scaling the wave number axis $k$ by a factor $\xi^{-2}\lambda$ to remove the time dependence from $I_0$, the argument of the exponential becomes

$$-(4\pi^2 + k^2\xi^{-4}\lambda^4)\frac{\xi^2}{4\lambda^2} = -\left(\frac{\pi^2\xi^2}{\lambda^2} + \frac{k^2\lambda^2}{4\xi^2}\right).$$

Since $\xi(t)$ and $\lambda(t)$ have a different time dependence, in general, the argument of the exponential still depends on time. However, in the special case where $\xi(t)$ and $\lambda(t)$ have the same time dependence, i.e., $\xi(t) \propto \lambda(t)$, the ratio $\xi\lambda^{-1}$ is time independent and the PSD would simplify to, scaling the vertical PSD axis by a factor $2w^{-2}\xi^{-2}$,

$$Q(k) = \exp\left[-\left(\pi^2 + \frac{k^2}{4}\right)\right] I_0(\pi k), \tag{9}$$

which is independent of time. Thus, the PSD of a mounded surface only exhibits time-dependent scaling when $\xi(t) \propto \lambda(t)$ or, using the definitions of the time-dependent behaviors of the lateral correlation length and wavelength from Eqs. (4) and (8), when $p = 1/z$. Since the time-dependent scaling of the PSD was shown to be a consequence of dynamic scaling in Sec. II B, mounded surfaces should not obey dynamic scaling when $p \neq 1/z$.

## IV. EXPERIMENTS

To observe the breakdown of dynamic scaling under shadowing growth, surfaces have been deposited using sputter deposition and chemical vapor deposition. Both of these deposition techniques introduce an angular flux on the substrate that is required for shadowing to take place. In addition, silicon was used as a source material because silicon films, under suitable deposition conditions, can be made amorphous. Crystalline effects were ignored in the MC simulations, so amorphous films are needed to compare simulation results to experiment.

### A. Sputter deposition

A dc magnetron sputtering system was used to deposit amorphous Si on an initially flat Si(100) substrate. In all depositions, a power of 200 W and an Ar pressure of $2.0 \times 10^{-3}$ Torr was used. Depositions ranging from 7.5 to 960 min were performed at a deposition rate of ~8 nm/min. The surfaces were imaged using atomic force microscopy (AFM), and images of these surface profiles are given in Fig. 3. For each deposition, statistics from four different AFM scans have been averaged, and the results are depicted in Fig. 4. The analysis gives $p = 0.51 \pm 0.03$, $1/z = 0.38 \pm 0.03$, $\beta = 0.55 \pm 0.09$, and $\alpha = 0.69 \pm 0.09$. Even though shadowing is

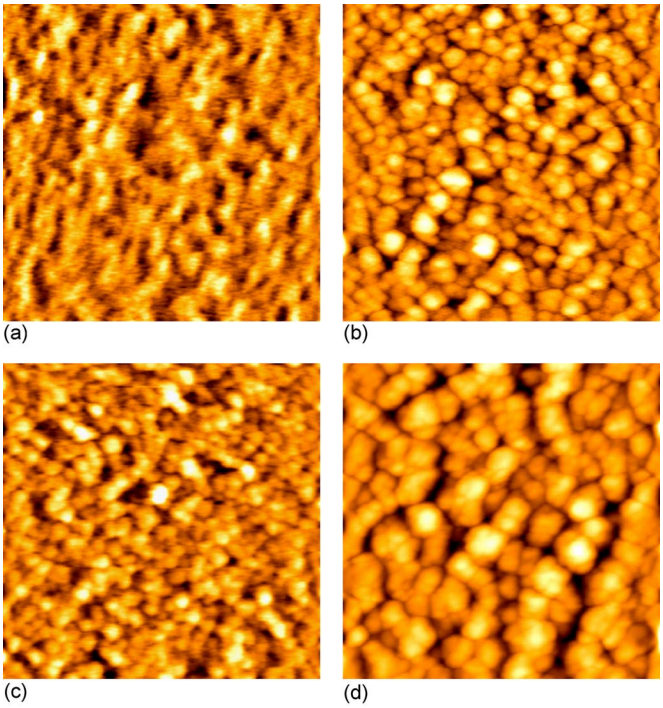


FIG. 3. (Color online) Atomic force microscopy (AFM) images of sputtered Si on Si at various deposition times: (a) $t = 7.5$ min (0.5 $\mu$m × 0.5 $\mu$m), (b) $t = 30$ min (1 $\mu$m × 1 $\mu$m), (c) $t = 240$ min (2 $\mu$m × 2 $\mu$m), and (d) $t = 960$ min (3 $\mu$m × 3 $\mu$m). The size of each image is given in parentheses.

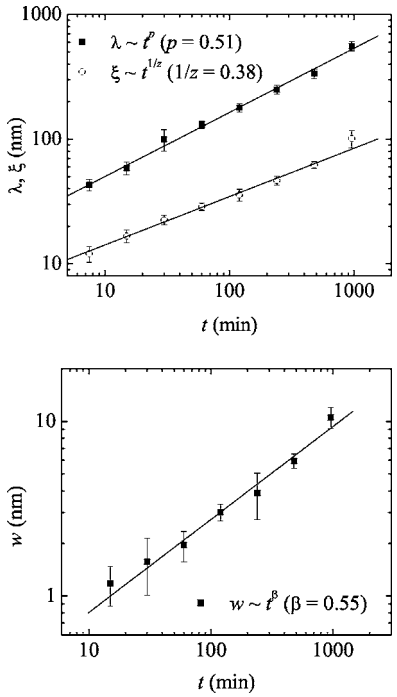


FIG. 4. Measured data for the wavelength $\lambda$, lateral correlation length $\xi$, and interface width $w$ for sputtered Si on Si (see Fig. 3). The extracted values for the exponents are $p = 0.51 \pm 0.03$, $1/z = 0.38 \pm 0.03$, and $\beta = 0.55 \pm 0.09$.

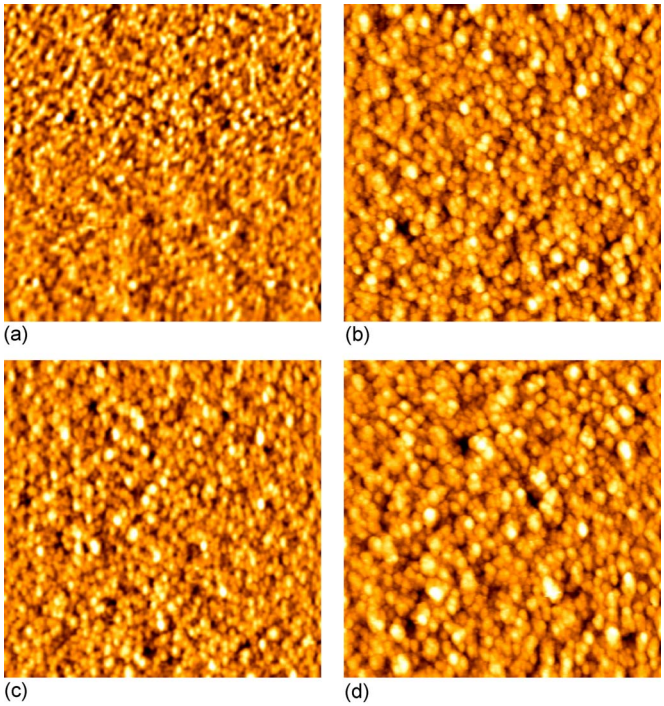


FIG. 5. (Color online) Atomic force microscopy (AFM) images of PECVD SiN at various deposition times: (a) $t=10$ min, (b) $t=45$ min, (c) $t=90$ min, and (d) $t=120$ min. The size of each image is 2 $\mu$m$\times$2 $\mu$m.

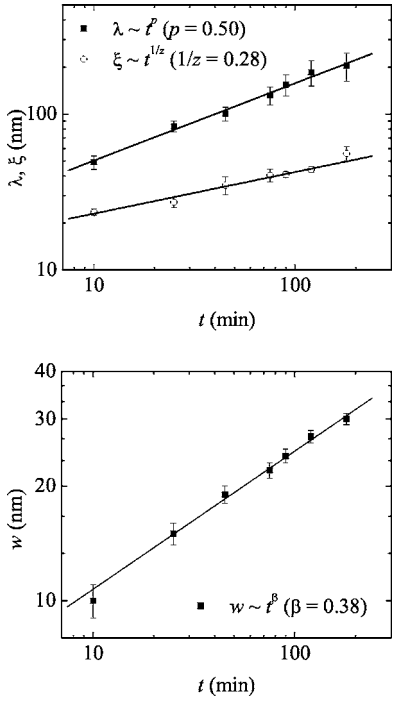


FIG. 6. Measured data for the wavelength λ, lateral correlation length $\xi$, and interface width $w$ for PECVD SiN (see Fig. 5). The extracted values for the exponents are $p=0.50\pm0.06$, $1/z=0.28\pm0.02$, and $\beta=0.38\pm0.02$.

present in this deposition, $\beta<1$ because reemission is also significant. The values of $p$, $1/z$, $\beta$, and $\alpha$ are consistent with the results of MC simulations with a sticking coefficient $s_0 \approx 0.65$, well within the regime of wavelength selection as predicted by simulation results. The value of $\alpha$ was measured from the height-height correlation function $H(r) \sim r^{2\alpha}$ for $r \ll \xi$, which is not depicted in Fig. 4.

### B. Chemical vapor deposition

In addition, amorphous SiN films have been deposited using a plasma enhanced CVD (PECVD) procedure.[16] The silicon nitride films were deposited in a Plasma-Therm™ Model 70 using a flow of $SiH_4/N_2/He$ mixtures to generate the plasma. The total deposition pressure was 0.89 Torr, the RF power was 32 W (which corresponds to 0.032 W/cm for this system), and the RF was 13.56 MHz. The flow rates for $SiH_4$, $N_2$, and He were 10, 478, and 1572 $cm^3$/min at STP, respectively. The front side of Si(100) wafers, which were RCA cleaned prior to deposition, were used as the substrate surface. Depositions were performed at a substrate temperature of 250 °C and times ranging from 10 to 180 min, with a growth rate of 4.70±0.07 nm/min.

The AFM images of the SiN surface profiles are given in Fig. 5. The time evolution of the wavelength λ, lateral correlation length $\xi$, and interface width $w$ are plotted in Fig. 6. The analysis gives $p=0.50\pm0.06$, $1/z=0.28\pm0.02$, $\beta=0.37\pm0.01$, and $\alpha=0.75\pm0.04$.

## V. MONTE CARLO SIMULATIONS

The solid-on-solid (2+1)-dimensional Monte Carlo (MC) simulations used in this research have been designed to mimic the growth of thin films by normal incidence deposition, chemical vapor deposition (CVD), and sputter deposition. In normal incidence deposition, the incident flux is uniformly normal to the surface, whereas for CVD and sputter deposition, the incident flux has an angular distribution of $\cos\theta$, where $\theta$ is defined with respect to the surface normal. A cosine flux distribution is typical of CVD and sputter deposition at higher working gas pressures, where the mean free path of incident particles is small compared to the geometrical dimensions of the source-substrate separation. The strength of surface diffusion can be controlled in the simulations and is represented by the variable $D/F$. $D$ represents the number of atoms available to diffuse per unit time, and $F$ represents the number of atoms deposited on the surface per unit time. Larger values of $D/F$ represent stronger surface diffusion. For a detailed description of the MC simulations used, see Karabacak *et al.*[19] The results of all MC simulations are summarized in Table I.

### A. Normal incidence deposition simulations

The shadowing effect is active only when there exists an angular distribution of incident particle flux. If there is no angular flux distribution, then taller surface features cannot block the incoming flux from the lower-lying areas of the surface, and shadowing is not effective. Thus, in normal incidence deposition, there is no shadowing because the incident flux is uniformly normal to the surface. In the normal incidence deposition simulations, from Table I, no wavelength selection is seen for all values of the sticking coefficient $s_0$, a direct result of the absence of shadowing.

TABLE I. Results of Monte Carlo simulations under normal incidence deposition and CVD and sputter deposition. Wavelength selection is absent from the normal incidence simulations, and only observed in the CVD and sputter simulations for larger values of the sticking coefficient ($s_0 \geq 0.5$).

| Flux | $s_0$ | $D/F$ | $p$ | $\beta$ | $\alpha$ | $1/z$ | $\beta/\alpha$ |
|---|---|---|---|---|---|---|---|
| CVD and sputter | 1.000 | 0 | 0.51±0.02 | 1.00±0.01 | 0.67±0.03 | 0.41±0.01 | 1.49±0.07 |
| | 1.000 | 20 | 0.50±0.02 | 1.00±0.01 | 0.59±0.01 | 0.40±0.04 | 1.69±0.03 |
| | 1.000 | 100 | 0.49±0.02 | 1.00±0.01 | 0.63±0.01 | 0.33±0.02 | 1.59±0.03 |
| | 1.000 | 200 | 0.50±0.02 | 1.00±0.01 | 0.55±0.02 | 0.36±0.02 | 1.82±0.07 |
| | 0.950 | 100 | 0.48±0.03 | 1.00±0.01 | 0.57±0.03 | 0.29±0.03 | 1.75±0.09 |
| | 0.875 | 100 | 0.48±0.02 | 1.00±0.01 | 0.51±0.03 | 0.28±0.03 | 1.96±0.12 |
| | 0.800 | 100 | 0.51±0.03 | 1.00±0.01 | 0.55±0.07 | 0.25±0.08 | 1.82±0.23 |
| | 0.750 | 100 | 0.45±0.03 | 1.00±0.01 | 0.43±0.03 | 0.16±0.07 | 2.33±0.16 |
| | 0.700 | 100 | 0.47±0.03 | 1.00±0.01 | 0.55±0.07 | 0.12±0.05 | 1.82±0.23 |
| | 0.625 | 100 | 0.48±0.04 | 0.58±0.03 | 0.63±0.03 | 0.40±0.03 | 0.92±0.06 |
| | 0.500 | 100 | 0.51±0.03 | 0.25±0.03 | 0.65±0.06 | 0.61±0.01 | 0.35±0.10 |
| | 0.375 | 100 | | 0.16±0.03 | 0.44±0.05 | 0.55±0.03 | 0.36±0.07 |
| | 0.250 | 100 | | 0.14±0.03 | 0.25±0.05 | 0.48±0.04 | 0.56±0.16 |
| | 0.125 | 100 | | 0.11±0.03 | 0.29±0.04 | 0.48±0.03 | 0.38±0.12 |
| Normal | 1.000 | 20 | | 0.45±0.02 | | | |
| | 0.750 | 100 | | 0.06±0.03 | 0.25±0.01 | 0.36±0.04 | 0.24±0.12 |
| | 0.500 | 100 | | 0.11±0.03 | 0.25±0.01 | 0.37±0.07 | 0.44±0.12 |
| | 0.250 | 100 | | 0.08±0.03 | 0.25±0.01 | 0.33±0.04 | 0.32±0.12 |

### B. CVD and sputter deposition simulations

Once an angular distribution of flux is introduced, as in the CVD and sputter deposition simulations, wavelength selection is clear. Figure 7 shows simulated surface profiles for the CVD and sputter deposition MC simulation with $s_0=1$. Figure 8 contains a plot of the wavelength λ as a function of time for this simulation, where the wavelength exponent $p=0.49\pm0.02$. The time scale used is defined such that one time step corresponds to approximately 50 deposited particles per surface point on average. The simulations were run on a $512\times512$ lattice up to a simulation time $t=20$. From Table I, when the sticking coefficient $s_0$ is reduced in the simulations, the value of the wavelength exponent remains relatively constant at $p\approx0.5$. However, once the sticking coefficient is sufficiently small ($s_0<0.5$), the reemission effect is strong enough to redistribute a significant amount of particle flux to otherwise shadowed surface features, which effectively cancels the shadowing effect and eliminates wavelength selection. Also, from Table I, varying the strength of surface diffusion ($D/F$) does not have a significant effect on the growth exponents. Since diffusion is a local growth effect, it is not as strong as the nonlocal shadowing effect and has negligible influence on the growth exponents when shadowing is present.

The behavior of the dynamic exponent $1/z$ in the CVD and sputter deposition simulations is significantly different from the wavelength exponent $p$. From Table I, the dynamic exponent $1/z$ can lie between 0.12 to 0.61 depending on the sticking coefficient, whereas the wavelength exponent $p\approx0.5$ whenever there is wavelength selection. The fact that the wavelength exponent is independent of sticking coefficient (for $s_0>0.5$) could suggest that these mounded surfaces may have a "universal" behavior when regarding wavelength selection. However, there is clearly no such universal behavior for the evolution of the lateral correlation length governed by the exponent $1/z$, which depends strongly on the sticking coefficient from the MC simulations. Experimentally, the value of $1/z$ reported in the literature scatters between 0.13 and 0.85.[14,16,19–25] Therefore, it is reasonable to believe that the value of $1/z$ is not universal and strongly depends on deposition conditions.

In addition, the growth exponent $\beta$ associated with the temporal evolution of the interface width behaves in a manner consistent with shadowing. When the shadowing effect is dominant in the MC simulations, $\beta=1$, consistent with theoretical results.[18] Also, simulation results predict that reemission begins to become significant when $s_0\approx0.7$, at the point where $\beta$ begins to decrease. Since reemission tends to smoothen the surface, strong reemission will slow the growth of the vertical roughness of the surface, thereby decreasing the value of $\beta$. Reemission becomes the dominant growth effect when $s_0<0.5$, where the surface is no longer mounded due to a lack of wavelength selection.

## VI. DISCUSSION

The most important result of these simulations and experimentally deposited surfaces is that $p\neq1/z$, in general, and the PSD of the surface profiles should not scale in time. This behavior is clearly seen in Fig. 9(a), which contains various PSD curves extracted at different stages in the evolution of surfaces created in the CVD and sputter deposition MC

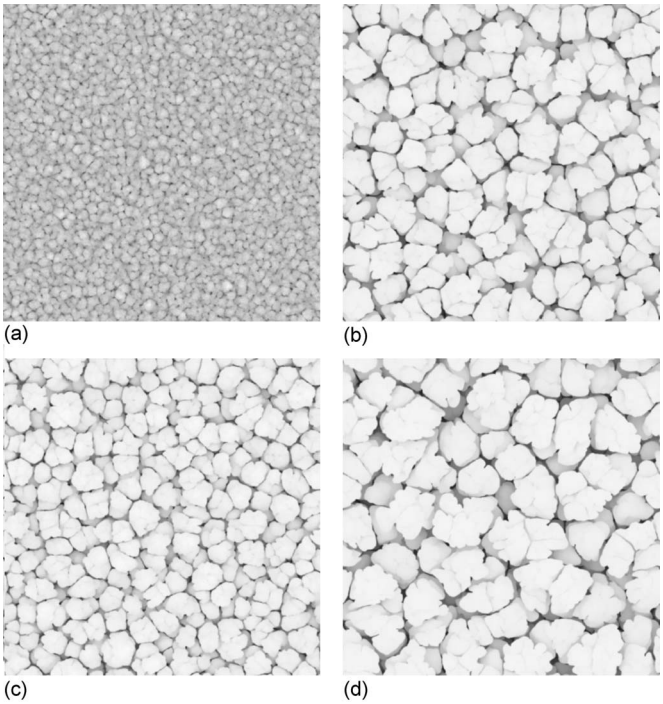


FIG. 7. Simulated surface profiles under CVD and sputter deposition flux with sticking coefficient $s_0=1$. The deposition time $t$ is defined such that one time step corresponds to an average of 50 deposited particles per lattice point. (a) $t=1$, (b) $t=6$, (c) $t=12$, and (d) $t=20$. The size of each image is $512\times512$ lattice units.

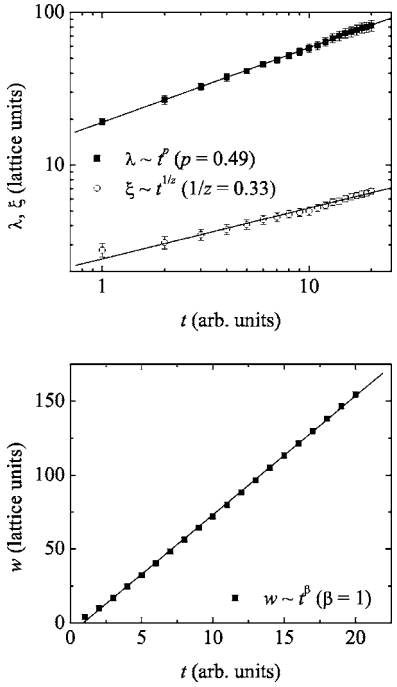


FIG. 8. Measured data for the wavelength λ, lateral correlation length $\xi$, and interface width $w$ for the CVD and sputter deposition MC simulation with sticking coefficient $s_0=1$ (see Fig. 7). The extracted values for the exponents are $p=0.49\pm0.02$, $1/z=0.33\pm0.02$, and $\beta=1.00\pm0.01$.

simulation with $s_0=1$. A similar plot is shown in Fig. 9(b) measured from sputtered Si surfaces described earlier. The PSD curves are scaled so their peaks coincide, which results in the wave-number axis multiplied by a factor of $\lambda\sim t^p$. Since the peak position defines the value for the wavelength, scaling the peaks of the curves corresponds to scaling the surfaces according to long-range (small-wave-number) behavior. A clear deviation is observed in the spread of the curves. The behavior of the PSD for larger wave numbers corresponds to the short-range behavior of the surface as represented by the lateral correlation length. Since $p\neq1/z$ for these surfaces, these length scales do not evolve at the same rate, which leads to the behavior seen in Fig. 9. In the scaled curves, the spread is proportional to $t^{-1/z}t^p=t^{p-1/z}$, and since $p>1/z$ in these examples, the widths of the scaled curves increase with time. It follows that measuring different values for the exponents $p$ and $1/z$ is evidence of the breakdown of dynamic scaling for mounded surfaces, as has been shown in both simulations and experimentally deposited mounded surfaces. Therefore, in general, the nonlocal effects that lead to mound formation do not allow the system to scale and the system loses its dynamic scaling behavior.

In addition, from Sec. II B, when a surface obeys dynamic scaling, the growth exponents are related in a specific way, namely, $1/z=\beta/\alpha$. This relation should no longer hold for surfaces grown under the influence of shadowing because dynamic scaling no longer holds for these surfaces. For the experimental sputter deposition,

$$\frac{1}{z}=0.38\pm0.03,\quad \frac{\beta}{\alpha}=0.80\pm0.17,$$

which do not agree within experimental error. Also, for the experimental CVD,

$$\frac{1}{z}=0.28\pm0.02,\quad \frac{\beta}{\alpha}=0.49\pm0.03,$$

which also do not agree within experimental error. For the MC simulation results in Table I, the last two columns of the table give values for $1/z$ and $\beta/\alpha$, respectively, for comparison. Note that when wavelength selection is dominant (for $s_0\geq0.5$), there is a significant difference between $1/z$ and $\beta/\alpha$. However, when reemission is strong enough to cancel wavelength selection, $1/z\approx\beta/\alpha$ within experimental error. Similarly for the normal incidence simulations, there is no wavelength selection as a result of the absence of the shadowing effect, and once again $1/z\approx\beta/\alpha$ within experimental error. These results suggest that when the shadowing effect is sufficiently suppressed during deposition, the surface obeys the dynamic scaling hypothesis. Note that simply investigating the validity of the relation $1/z=\beta/\alpha$ is not sufficient to claim a breakdown of dynamic scaling alone. It is simply an observation that logically follows when dynamic scaling has been broken, as a result of $p\neq1/z$ under shadowing.

An analysis of the one-dimensional profile of the growth front gives further insight into the breakdown of dynamic scaling under shadowing. Figure 10 includes a one-dimensional profile view of a simulated CVD and sputter

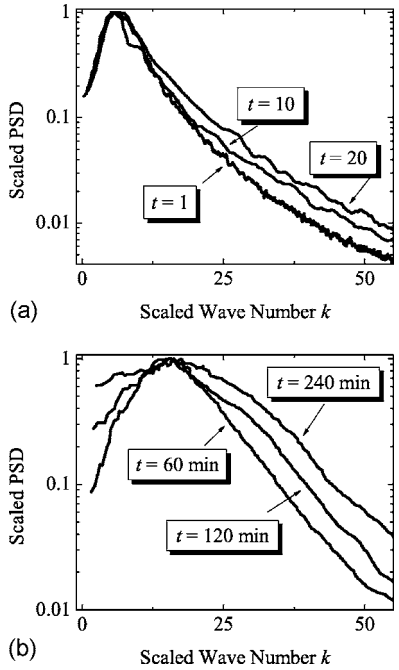


FIG. 9. (a) Rescaled PSD curves for the CVD and sputter deposition MC simulation with sticking coefficient $s_0=1$. The curves are scaled according to peak position, which scales the long-range (small $k$) behavior of the PSD. The overall spread of the curves (large $k$) does not scale, evidence of a breakdown of dynamic scaling. (b) Rescaled PSD curves for experimentally deposited sputter Si on Si.

deposited surface with sticking coefficient $s_0=1$. The profile includes a number of sharp valleys that are formed under the influence of shadowing. We purposely choose the case of sticking coefficient $s_0=1$ to display the effect more prominently. As a result of the presence of these valleys, the mound size may evolve at a different rate than the mound separation, which leads to the breakdown of dynamic scaling.

In the MC simulations and experimental surfaces studied in this work that exhibit wavelength selection, the wavelength exponent $p\approx 0.5$ when wavelength selection is present, which suggests that the growth process responsible for the value of the wavelength exponent is common to all depositions analyzed in this work. One such growth effect is the noise inherent to the deposition. In the MC simulations, the shot noise $\eta(\mathbf{r},t)$ was assumed to have a Gaussian distribution, with $\langle \eta(\mathbf{r},t)\rangle=0$ and $\langle \eta(\mathbf{r},t)\eta(\mathbf{r}',t')\rangle=2D\delta^d(\mathbf{r}-\mathbf{r}')\delta(t-t')$. A closer analysis of the shadowing effect suggests that the shot noise is required for shadowing to take place when the initial surface is flat. The shadowing effect is a result of the competition between surface features of different heights to receive incident particle flux. The noise in the system allows some surface features to randomly grow taller than others, which leads to shadowing. Without noise, starting from a flat substrate, no surface heights would preferentially grow taller than others, eliminating shadowing. This suggests that the nature of the noise in the system has an effect on the value of the wavelength exponent.

A theoretical argument for $p=1/2$ can be constructed using results of Meakin and Krug.[26] For a $(1+1)$-dimensional

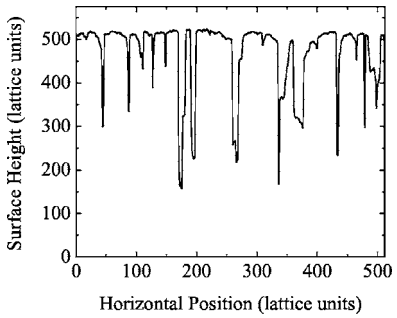


FIG. 10. One-dimensional profile view of a simulated CVD and sputter deposited surface with sticking coefficient $s_0=1$.

surface grown under shadowing, ignoring lateral growth on the surface, Meakin and Krug showed that the linear concentration of unshadowed mounds $c(t)$ behaves as

$$c(t)\sim t^{-1/2}. \tag{10}$$

This result is derived from the condition that unshadowed mounds grow according to a Poisson process, which implies that individual mound heights perform a random walk about their mean. This is a reasonable assumption because unshadowed mounds experience the full incident particle flux, which is subject to a Gaussian noise distribution.

Using a simple geometric argument, $c(t)$ can be related to the wavelength $\lambda$. For a $(1+1)$-dimensional surface, if the surface is of linear size $L$, and the average distance between mounds is $\lambda$, then there are $L/\lambda$ mounds on the surface. Similarly, by the definition of $c(t)$, there are $c(t)L$ mounds on the surface. This implies that $c(t)L\sim L/\lambda$, or

$$c(t)\sim \lambda^{-1}, \tag{11}$$

from which $p=1/2$ follows. A similar argument holds in $2+1$ dimensions, recalling that $c(t)$ is a linear density of mounds. The total number of mounds on the surface can be represented as $[c(t)L]^2$ and $(L/\lambda)^2$ in $2+1$ dimensions, which again leads to $p=1/2$.

Even though this argument correctly predicts that $p=1/2$, it is based on a model that ignores the lateral growth of mounds or, similarly, ignoring the lateral correlation length governed by the exponent $1/z$. However, from simulation results, the behavior of $p$ and the behavior of $1/z$ do not appear to be correlated under different deposition conditions. It therefore seems reasonable that $p$ and $1/z$ are independent in this context, with $p$ determined by the shot noise and $1/z$ determined by deposition conditions, such as the sticking coefficient and strength of diffusion. This argument is far from a proof for the general behavior of the wavelength exponent $p$, and further work is needed to fully quantify the behavior of the wavelength exponent under various deposition conditions.

Previous study on the effects of shadowing[5,6] and reemission[8] did not examine quantitatively the behavior of the time evolution of the wavelength $\lambda$. It is important to note that some authors have used the variable $p$ to describe the time evolution of the lateral correlation length as opposed to wavelength selection. Using a model based on the Huy-

gens principle (HP), Tang *et al.*[5] examined the evolution of the lateral correlation length $\xi$ of simulated surfaces. The exponent $1/z$ associated with the lateral correlation length depends on the initial surface configurations and ranges from 1/4 to 1. However, under the HP, mounds grow next to each other without gaps and the spacing between mounds is the same as the mound size, or $\xi=\lambda$, which implies $p=1/z$. A continuum model presented in Yao and Guo[6] accounted for shadowing during the growth process, which predicted $1/z=0.33$, consistent with simulation results under the specific condition of $s_0=1$. Yao *et al.* extracted the growth exponent of the columnar structures in their simulated surfaces by scaling regions of the PSD.[7] Their scaling was of the spread of the PSD, not the peak; thus, the value they obtained by scaling arguments corresponds to the value of $1/z$ in the present work, not the value of the wavelength exponent $p$. Only the behavior of the exponent $1/z$ was investigated in their work and, as a result, since $p \neq 1/z$, in general, the peaks of scaled PSD curves in their work do not coincide.

It is noted that previous work on the behavior of surfaces grown under a step diffusion barrier utilized similar analysis techniques to those used in this work. In particular, Siegert[27] showed that, under certain conditions in MBE growth, the surface can be quantified by two length scales that do not evolve at the same rate, similar to the discussion of the wavelength $\lambda$ and correlation length $\xi$ discussed in this paper. Also, Moldovan and Golubovic[28] showed that, for simulated surfaces grown under step-barrier diffusion, the height-height correlation function does not exhibit time-dependent scaling. Since the PSD can be related to the Fourier transform of the height-height correlation function, analyzing the time-dependent scaling behavior of the height-height correlation function is similar to analyzing the time-dependent scaling behavior for the PSD. However, both these papers focused solely on step-barrier diffusion, which can be modeled by a local continuum equation. The shadowing and reemission effects studied in this work are nonlocal and lead to a markedly different surface morphology than is created in step-barrier diffusion.

## VII. CONCLUSION

In conclusion, a study of mound formation under shadowing during thin film growth has been presented. The wavelength exponent $p$ can be used to characterize the evolution of mounds on the film, defined in terms of the time evolution of the peak position of the PSD, $k_m \sim t^{-p}$. For the surfaces studied in this work, $p \approx 0.5$, independent, within error, of the strength of reemission and diffusion. A comparison of the average mound separation $\lambda$ and lateral correlation length $\xi$ reveals that their behavior is not necessarily the same, evidence that the entire system does not dynamically scale. From this analysis, thin film deposition appears to be much more complex than originally anticipated due to nonlocal effects. However, the evolution of the wavelength that characterizes the separation of mounds appears to be universal.

## ACKNOWLEDGMENTS

M.P. was supported by the NSF Research Experience for Undergraduates (Grant No. REU PHY 0353163) and Undergraduate Research Program (URP) at Rensselaer. C.G. was supported by NSF Grant No. CMS 0324492.

[1] F. Family and T. Vicsek, J. Phys. A **18**, L75 (1985).
[2] F. Family, J. Phys. A **19**, L441 (1986).
[3] P. Meakin, *Fractals, Scaling, and Growth Far from Equilibrium* (Cambridge University Press, Cambridge, England, 1998), p. 401.
[4] A.-L. Barabasi and H. E. Stanley, *Fractal Concepts in Surface Growth* (Cambridge University, Cambridge, England, 1995).
[5] C. Tang, S. Alexander, and R. Bruinsma, Phys. Rev. Lett. **64**, 772 (1990).
[6] J. H. Yao and H. Guo, Phys. Rev. E **47**, 1007 (1993).
[7] J. H. Yao, C. Roland, and H. Guo, Phys. Rev. A **45**, 3903 (1992).
[8] Y.-P. Zhao, J. T. Drotar, G.-C. Wang, and T.-M. Lu, Phys. Rev. Lett. **87**, 136102 (2001).
[9] For review, see P. Politi, G. Grenet, A. Marty, A. Ponchet, and J. Villain, Phys. Rep. **324**, 271 (2000).
[10] M. D. Johnson, C. Orme, A. W. Hunt, D. Graff, J. Sudijono, L. M. Sander, and B. G. Orr, Phys. Rev. Lett. **72**, 116 (1994).
[11] P. E. Hegeman, H. J. W. Zandvliet, G. A. M. Kip, and A. van Silfhout, Surf. Sci. **311**, L655 (1994).
[12] J.-K. Zuo and J. F. Wendelken, Phys. Rev. Lett. **78**, 2791 (1997).
[13] M. Pelliccione, T. Karabacak, and T.-M. Lu, Phys. Rev. Lett. **96**, 146105 (2006).
[14] Y.-P. Zhao, G.-C. Wang, and T. M. Lu, *Characterization of Amorphous and Crystalline Rough Surface: Principles and Applications* (Academic Press, New York, 2001), p. 38.
[15] T. Michely and J. Krug, *Islands, Mounds, and Atoms: Patterns and Processes in Crystal Growth Far from Equilibrium* (Springer, New York, 2003).
[16] T. Karabacak, Y.-P. Zhao, G.-C. Wang, and T.-M. Lu, Phys. Rev. B **66**, 075329 (2002).
[17] T.-M. Lu, Y.-P. Zhao, J. T. Drotar, T. Karabacak, and G.-C. Wang, in *Morphological and Compositional Evolution of Thin Films*, edited by M. J. Aziz, N. C. Bartelt, I. Berbezier, J. B. Hannon, and S. J. Hearne, MRS Symposia Proceedings No. 749 (Materials Research Society, Pittsburgh, 2003), p. 3.
[18] Jason T. Drotar, Y.-P. Zhao, T.-M. Lu, and G.-C. Wang, Phys. Rev. B **62**, 2118 (2000).
[19] T. Karabacak, Y.-P. Zhao, G.-C. Wang, and T.-M. Lu, Phys. Rev. B **64**, 085323 (2001).
[20] D. R. Luhman and R. B. Hallock, Phys. Rev. Lett. **92**, 256102 (2004).
[21] P. Jain, J. S. Juneja, T. Karabacak, E. J. Rymaszewski, and T.-M. Lu, in *Morphological and Compositional Evolution of Thin Films*, edited by M. J. Aziz, N. C. Bartelt, I. Berbezier, J. B. Hannon, and S. J. Hearne, MRS Symposia Proceedings No. 749 (Materials Research Society, Pittsburgh, 2003), p. 107.
[22] F. Ojeda, R. Cuerno, R. Salvarezza, and L. Vazquez, Phys. Rev. Lett. **84**, 3125 (2000).

[23] C. V. Dharmadhikari, A. O. Ali, N. Suresh, D. M. Phase, S. M. Chaudhari, A. Gupta, and B. A. Dasannacharya, Mater. Sci. Eng., B **75**, 29 (2000).
[24] D. M. Tanenbaum, A. L. Laracuente, and A. Gallagher, Phys. Rev. B **56**, 4243 (1997).
[25] M. Lutt, J. P. Schlomka, M. Tolan, J. Stettner, O. H. Seeck, and W. Press, Phys. Rev. B **56**, 4085 (1996).
[26] P. Meakin and J. Krug, Phys. Rev. A **46**, 4654 (1992).
[27] M. Siegert, Phys. Rev. Lett. **81**, 5481 (1998).
[28] D. Moldovan and L. Golubovic, Phys. Rev. E **61**, 6190 (2000).